Impulse Response Generation from *S*-Parameters for Power Delivery Network Simulation

Ilgweon Kang[†], Xinan Wang[†], Jeng-Hau Lin[†], Ryan Coutts[‡] and Chung-Kuan Cheng[†‡]
[†]CSE and [‡]ECE Departments, UC San Diego, La Jolla, CA 92093
{igkang, xinan, jel252, rmcoutts, ckcheng}@ucsd.edu

***Abstract*—Accurate analysis of power delivery network is indispensable to assess VLSI package and interconnection network. Given the *S*-parameters that characterize the linear packaging system, we derive the transient response of power delivery networks. We utilize the compressed sensing technique to generate the impulse response that fits the *S*-parameters with sparsity. Our method shows accurate, concise, and stable results.**

I. Introduction

Package-level simulation for power delivery network (PDN) is an important procedure to assess microelectronic design quality. As high-speed data processing becomes contemporary trends, massive signal traffic may induce undesired impact on power integrity. Usually, the characterization of the PDN network relies on the specification in frequency domain, e.g., *S*-parameters, while the simulation of the system is performed in time domain. Therefore, the conversion from frequency domain description to time domain information is essential for the PDN network analysis.

Previous efforts to translate the frequency domain description are categorized into two groups by computational procedure; (1) the direct generation of impulse responses [1], [2], [12] and (2) the extraction of macromodels which are compatible to SPICE netlist [13]. The first approach performs a direct conversion from frequency domain to time domain and thus has the potential to minimize the conversion error. However, the usage of the impulse response requires convolution in time for transient simulation which causes a complexity of $O(n^2)$ where n is the number of sample points in time. In [11], Peng and Cheng dropped the complexity of convolution method to $O(nlog^2n)$ utilizing a hierarchical approach and demonstrated the efficiency of the direct approach.

For the direct impulse response generation, one key issue of the *S*-parameter is that the specification may contain much fewer samples than the amount required by the Shannon-Nyquist sampling theorem [10]. Suppose that the *S*-parameter file covers samples at all frequency range, then an inverse Fourier transform will derive the corresponding time domain information. However, in practice, the *S*-parameter file includes very limited amount of samples only at frequencies of main interests. In [12], Rao optimized the spectrum beyond the specified samples to reduce the error from the samples with the causality constraint. The passivity is enforces by scaling the eigenvalues of the scattering matrix at where the passivity constraint is violated.

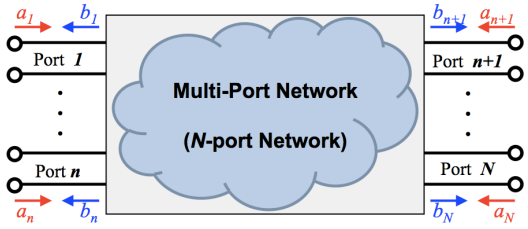

Fig. 1: A multi-port network with incident and reflected power waves.

In this paper, we adopt a compressed sensing method for the impulse response generation. The compressed sensing method is a signal processing technique which has been used to recover solutions from undetermined linear system, e.g., image processing. We select a set of wavelets to construct the impulse response. Our goal is to find a sparse list of the wavelets that fits the *S*-parameters.

Our main contributions can be summarized as follows.

- We adopt a compressed sensing method to convert the *S*-parameters into impulse responses.
- We select the set of wavelets to fit the impulse responses of PDN networks.
- We show that the proposed method derive accurate, concise, and stable results although the given dataset is sparse and deficient.

In the remainder of this paper, section II introduces preliminaries and constraints to obtain physically consistent models. Section III describes the problem formulation in detail, and section IV shows experimental results that verify the proposed method with compressed sensing technique. Finally, Section V presents the ongoing work and concludes the paper.

II. *S*-Parameters and Constraints

A. *S*-parameters

Figure 1 illustrates a multi-port system, where *scattering coefficients* a_i and b_i denote respectively the incident and reflected *power waves* at port i for $1 \leq i \leq N$. The scattering matrix has its element determined as $S_{ij} = b_i/a_j$ when $a_k = 0$ for all $k \neq j$. Thus, we have

$$\mathbf{b} = \begin{bmatrix} b_1 \\ \vdots \\ b_N \end{bmatrix} = \begin{bmatrix} S_{11} & \cdots & S_{1N} \\ \vdots & \ddots & \vdots \\ S_{N1} & \cdots & S_{NN} \end{bmatrix} \cdot \begin{bmatrix} a_1 \\ \vdots \\ a_N \end{bmatrix} = \mathbf{S} \cdot \mathbf{a}. \quad (1)$$

978-1-4799-1993-2/15/$31.00 ©2015 IEEE

B. Causality and Passivity Constraints

A PDN network in package is supposed to observe the causality and passivity constraints.

Causality: A linear time-invariant (LTI) system with a known delay τ is *causal* if the transfer function $f(t) = 0$ for $t < \tau$. To guarantee causality, the real part and imaginary part of a frequency response should satisfy *Kramers-Kronig relations* [8]. To simplify the following discussion, let us assume that $\tau = 0$. A causal function can be decomposed into an even and odd functions, i.e., $f(t) = f_e(t) + f_o(t)$, where $f_e(t)$ and $f_o(t)$ are even and odd parts of $f(t)$, respectively and $f_o(t) = sgn(t) \cdot f_e(t)$. Thus, we can write $f(t) = f_e(t) + sgn(t) \cdot f_e(t)$. By converting $f(t)$ to the frequency domain, we have

$$F(s) = F_e(s) - \frac{j}{\pi s} * F_e(s) = F_e(s) - j\widehat{F_e}(s). \tag{2}$$

where $\widehat{F}(s) = F(s) * \frac{1}{\pi s} = \frac{1}{\pi}\int_{-\infty}^{\infty} \frac{F(s')}{s-s'} ds'$ is the *Hilbert transform* of $F_e(s)$ [8]. In other words, the real and imaginary parts of scattering matrix have to observe the Hilbert transform relation to ensure the causality [8].

Passivity: The PDN network in package is passive and thus for every frequency its scattering matrix observes the following inequality [8].

$$\mathbf{a}^*\mathbf{a} \geq \mathbf{b}^*\mathbf{b} \tag{3}$$

where the superscript * denotes the conjugate transpose of the vector. Substituting Equation (1) into Equation (3), we have

$$\mathbf{a}^*\mathbf{a} - \mathbf{S}^*\mathbf{a}^*\mathbf{S}\mathbf{a} = \mathbf{a}^*(\mathbf{I} - \mathbf{S}^*\mathbf{S})\mathbf{a} \geq 0. \tag{4}$$

Therefore, the necessary and sufficient condition of passivity is that $0 \leq \lambda_i \leq 1$ for all eigenvalues λ_i of square matrix $\mathbf{S}^*\mathbf{S}$ [13].

We derive the passivity constraint in time-domain using discrete time points. We express the input $x(t)$ and output $y(t)$ with vectors $\mathbf{x} = [x(0),\ x(\Delta),\ \cdots,\ x(N\Delta)]^T$ and $\mathbf{y} = [y(0),\ y(\Delta),\ \cdots,\ y(N\Delta)]^T$, respectively, where Δ is the length of time step and the total time is $T = N \cdot \Delta$. The convolution of the impulse response $h(t)$ is written as matrix and vector multiplication.

$$\mathbf{y} = \mathbf{H} \cdot \mathbf{x} \tag{5}$$

where

$$\mathbf{H} = \begin{bmatrix} h(0) & 0 & \cdots & 0 \\ h(\Delta) & h(0) & \cdots & 0 \\ \vdots & \vdots & \ddots & \vdots \\ h(N\Delta) & h((N-1)\Delta) & \cdots & h(0) \end{bmatrix}. \tag{6}$$

The system is passive if and only if the following inequality holds for every possible input vector $\mathbf{x}$.

$$\mathbf{x}^T \cdot \mathbf{x} \geq \mathbf{y}^T \cdot \mathbf{y} \tag{7}$$

Substituting Equation (5) into Equation (7), we have

$$\mathbf{x}^T \cdot \mathbf{x} - \mathbf{x}^T \cdot \mathbf{H}^T \cdot \mathbf{H} \cdot \mathbf{x} \geq 0$$
$$\mathbf{x}^T \cdot [I - \mathbf{H}^T \cdot \mathbf{H}] \cdot \mathbf{x} \geq 0. \tag{8}$$

Therefore, we can summarize the condition of the passivity with the following theorem.

Theorem of passivity in time domain: A linear system is *passive* if and only if all eigenvalues of $\mathbf{H}^T\mathbf{H}$ locate in the interval $[0,1]$, i.e.,

$$I - \mathbf{H}^T \cdot \mathbf{H} \geq 0. \tag{9}$$

III. Compressed Sensing Approach

We now describe our approach using compressed sensing technique. In this section, we describe our formulation, algorithm and property of the approach.

A. Background

In order to obtain the accurate time-domain impulse response from the band-limited frequency-domain information, signal structure demands careful characterization. The *S*-parameters allow us to derive the frequency-domain counterpart of the time-domain impulse response. In principle, the sample points on frequency domain can reproduce the impulse response through applying the inverse Fourier transform. However, the characterization based on the inverse Fourier transform is not preferred by the intrinsic feature of the signal. For example, if a transmission line is concerned, the time delay and the sharp rising impulse response are important in the time domain features, which imply the existence of low frequency components as well as intensive information in relatively high frequency band. Therefore, the inverse Fourier transformation method based on insufficient frequency bandwidth would be insufficient to recover precise impulse response in the time domain.

B. Compressed Sensing Method

Compressed sensing is a signal processing technique that recovers a broad band signal from relatively less number of measurement. The approach relies on an assumption that the signal can be expressed with very sparse nonzero terms according to the basis of the representation [3]–[5].

C. Problem Formulation

Given a set of the scattering matrices at n sample (angular) frequencies $\omega_1,\ \cdots,\ \omega_n$, we have $\{S(\omega_1),\ \cdots, S(\omega_n)\}$. We recover the impulse response in the time domain by the linear combination of the wavelets $\psi_1(t),\ \cdots,\ \psi_m(t)$.

$$h(t) = \sum_i c_i \cdot \psi_i(t),\ (1 \leq i \leq m), \tag{10}$$

where c_i are the coefficients, $1 \leq i \leq m$.

We use two classes of wavelets.

(1) Morlet wavelets [9]:

$$\psi(t) = exp\left[-\frac{1}{2}(at)^2\right] \cdot (\cos\sigma t - K_\sigma) \tag{11}$$

where a and σ are adjustable parameters, and $K_\sigma = e^{-\frac{1}{2}\sigma^2}$. The Morlet wavelets have a trade-off between the exponential decay and infinite oscillation, both of which could be reproduced with extreme parameters of a and σ.

(2) Inverse Quadratic Polynomial (IQP) [7]:

$$\psi(t) = \begin{cases} \frac{1}{B^2+t^2} & \text{if } t \geq 0, \\ 0 & \text{otherwise,} \end{cases} \quad (12)$$

where B is a time derived from transmission line telegrapher's equation [7]. The IQP has a sharp rise at the beginning which is consistent with the impulse response of microelectronic packages.

Table I lists the parameters of the wavelets, which take values uniformly in its corresponding value interval. For example, parameter σ is taken in the interval $1-10$ with step length 1, and parameter a has multiple segments of intervals with different step lengths. We normalize the time interval to $[0,\ L]$ where $L = 10$. Furthermore, each wavelet is shifted along the time axis by the offset Δ_t to constitute the set of wavelets for our method.

TABLE I: Parameters for the wavelets bases.

Variable	Range	Interval
σ	1 - 10	1
Δ_t	0 - 5	0.05
a	0 - 2^0	2^{-3}
	2^0 - 2^4	2^0
	2^4 - 2^7	2^4
	2^7 - 2^{10}	2^7
B^2	0 - 2^{-7}	2^{-10}
	2^{-7} - 2^{-3}	2^{-7}
	2^{-3} - 2^0	2^{-3}

Each wavelet $\psi_i(t)$ is mapped via numerical Fourier transform to frequency domain to generate the template $\psi_i(\omega_j)$ at frequency ω_j. In order to fit the given S-parameters, i.e., to determine the coefficients c_i in Equation (10), we have the Equation (13).

$$\mathbf{A}_{2n\times m} \cdot \mathbf{c}_{m\times 1} = \mathbf{S}_{2n\times 1} \quad (13)$$

where $\mathbf{A}_{2n\times m}$ is the template matrix

$$\begin{bmatrix} \Psi_1(\omega_1)_R & \Psi_2(\omega_1)_R & \cdots & \Psi_m(\omega_1)_R \\ \Psi_1(\omega_2)_R & \Psi_2(\omega_2)_R & \cdots & \Psi_m(\omega_2)_R \\ \vdots & \vdots & \ddots & \vdots \\ \Psi_1(\omega_n)_R & \Psi_2(\omega_n)_R & \cdots & \Psi_m(\omega_n)_R \\ \Psi_1(\omega_1)_I & \Psi_2(\omega_1)_I & \cdots & \Psi_m(\omega_1)_I \\ \Psi_1(\omega_2)_I & \Psi_2(\omega_2)_I & \cdots & \Psi_m(\omega_2)_I \\ \vdots & \vdots & \ddots & \vdots \\ \Psi_1(\omega_n)_I & \Psi_2(\omega_n)_I & \cdots & \Psi_m(\omega_n)_I \end{bmatrix}, \quad (14)$$

the subscripts $(*)_R$ and $(*)_I$ represent the real part and the imaginary part of the input complex number, vector $\mathbf{c}_{m\times 1} = [c_1,\ \cdots,\ c_m]^T$, lists the coefficients in Equation (10) to be solved, and vector $\mathbf{S}_{2n\times 1} = [S(\omega_1)_R,\ \cdots,\ S(\omega_n)_R,\ S(\omega_1)_I,\ \cdots,\ S(\omega_n)_I]^T$.

The objective function is

$$\begin{aligned} \text{minimize} \quad & \| \mathbf{Ac} - \mathbf{S} \|_{L2}^2 \\ \text{subject to} \quad & \| \mathbf{c} \|_{L1} \leq N \end{aligned}$$

where N is a threshold to control the sparsity of our solution $\mathbf{c}$ [6]. We use $L1$ norm to produce sparse results, since $L0$ norm problem is NP-complete.

D. Algorithm

We adopt LARS method [6] to derive the optimal solution of $\mathbf{c}_{m\times 1}$ in Equation (13). Different methods have been proposed: the matching pursuit algorithm, the Lasso method, and the least angle regression (LARS) method. The matching pursuit algorithm is a greedy approach that approximates the target on each step by using the orthogonal projection onto the most correlated basis. The Lasso method adds the L_1-norm of the parameter vector as a constraint on the regression problem, and is expected to yield a more precise description in cost of computation. The least angle regression (LARS) method in [6] introduces a geometric insight in the selection process, which selects the most related basis one by one. Thereby, the number of bases can be directly controlled during the execution. It is less greedy than the matching pursuit algorithm. The LARS method generates the similar results with the Lasso method since the Lasso method that can be treated as a revised version of the LARS method; however, the LARS method is more efficient than the Lasso method up to orders of computation time.

Algorithm 1 presents the flow to generate impulse response $h(t)$ from frequency information. Lines 1-8 develop $\mathbf{A}_{2n\times m}$ and $\mathbf{S}_{2n\times 1}$ for LARS() function at Line 9, then we obtain $\mathbf{c}_{m\times 1}$. The wavelet approximation procedure is performed in Line 10.

Algorithm 1 The Flow to Generate Impulse Response

Procedure *GenImpResp*()
1: $\mathbf{S}_{2n\times 1} = [(sampleFreq.data)_R,\ (sampleFreq.data)_I]^T$;
2: **for all** wavelet ψ_i $(1 \leq i \leq m)$ **do**
3: **for all** sampling frequency ω_j $(1 \leq j \leq n)$ **do**
4: $FT_{i,j} = FourierTransform[\psi_i(t)]$ at ω_j;
5: **end for**
6: $\mathbf{A}_i = [(FT_{i,1})_R,\ \cdots,\ (FT_{i,n})_R,\ (FT_{i,1})_I,\ \cdots,\ (FT_{i,n})_I]^T$;
7: **end for**
8: $\mathbf{A}_{2n\times m} = [\mathbf{A}_1,\ \cdots,\ \mathbf{A}_m]$;
9: $\mathbf{c}_{m\times 1} = \text{LARS}(\mathbf{A}_{2n\times m},\ \mathbf{S}_{2n\times 1})$; // [15]
10: $h(t) = \sum_{i=1}^{m} (c_i \cdot \psi_i(t))$; // $h(t)$:Wavelet Approx. at t

E. Properties of Compressed Sensing Method

In this subsection, we describe the properties of compressed sensing in terms of causality, stability, and passivity.

Causality: For compressed sensing, the causality can be enforced by the selection of the wavelets. For a given propagation delay τ, we choose only the wavelet that is only nonzero after time $t \geq \tau$. However, the enforcement works only if the delay is known.

TABLE II: Commonly applied metrics to develop test cases.

Metal	Width	See Figure 2
	Length	15.000 inch
	Height	6.850E-4 inch
	Conductivity	5.8E+7
Substrate	Dielectric constant	4.2
	Thickness	0.010 inch
	Loss tangent	0.02

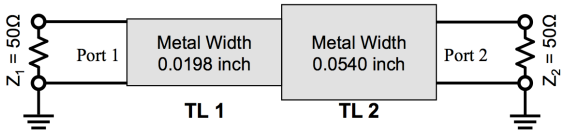

Fig. 2: Two-port transmission line test case; two microstrip lines cascaded (TL = Transmission Line).

Stability: The concept of stability is related to the boundedness of the system response. Mathematically, a system is *stable* if the output $y(t)$ is bounded for all bounded inputs $x(t)$ (BIBO) [8] [13]. In linear package, the stability is guaranteed if all the elements in the impulse response matrix **F** satisfy

$$\int_{-\infty}^{+\infty} \left| f_{ij}(t) \right| dt < +\infty. \tag{15}$$

For compressed sensing, the absolute integral of each wavelet is finite. Therefore, the absolute integral of the approximation as the combinations of the wavelets functions is also finite, which guarantees that the method is stable.

Passivity: The passivity can be observed by inequality (9). However, the incorporation of the constraint complicates the compressed sensing method. In this paper, we rely on the minimization of the $L1$ norm to reduce the power of the results.

IV. Experimental Results

We use the MATLAB code [15] to implement LARS method [6].

A. Test Case

1) Mismatched Transmission Lines: As shown in Figure 2, a transmission line with mismatched ends is designed for the verification of our compressed sensing based method. We extract the *S*-parameters as well as impulse responses of the test case with *Keysight Advanced Design System* [14] EDA tool. Table II presents the typical industrial metrics adopted to generate the test case. In Figure 2, the system has two-cascaded microstrip lines which have different metal widths to cover a multi-reflection due to the impedance mismatch.

In our test case, we assume that (1) the impedances of TL1 and TL2 are 50Ω and 25Ω, respectively, and (2) the substrate is FR4, which is the typical material for printed circuit board (PCB), and one inch equals to 1000mil. There are two mismatched interfaces; (1) the junction between the two segments and (2) the output port at port 2. We expect that the mismatched interfaces induce multi-reflections in the impulse response.

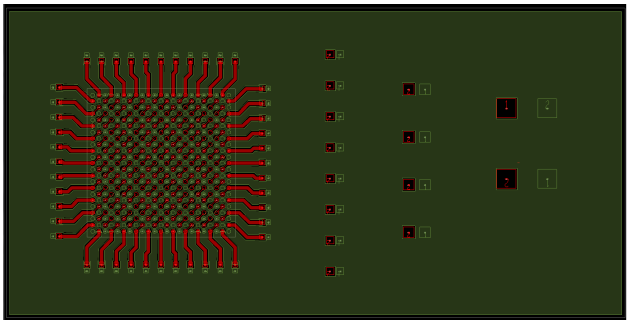

Fig. 3: A simple power distribution network.

2) Simple Power Distribution Network: The second test case is a simple power distribution network as shown in Figure 3. There are four kinds of decoupling capacitors for noise suppression. The capacitors from right to left and surrounding the die are 100uF in MLCC1206 (i.e., multilayer ceramic capacitor) package, 47uF in 0603, 4.7uF in 0402 and 1uF in 0201. The spacing between different capacitors is 0.1inch. The interested port is defined on the power pins of the die since the power integrity of the die is concerned. We expect the impulse response of this PDN to be small to suppress noise.

B. Experimental Results

1) Mismatched Transmission Lines: We verify our proposed method for generating the impulse responses by using the mismatched transmission line (i.e., shown in Figure 2). For the test case, we adopt 200 linearly spaced frequency sampling points ranging from 100MHz to 20GHz.

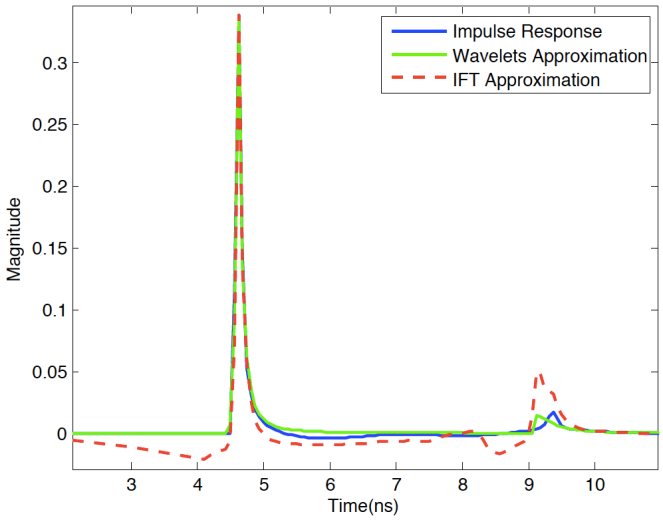

Fig. 4: Result of the mismatched test case in Figure 2. We can observe the multi-reflection on the impulse response. Our recovery based on wavelets shows significantly better performance than the inverse Fourier transform method in respect of preserving the delay and passivity.

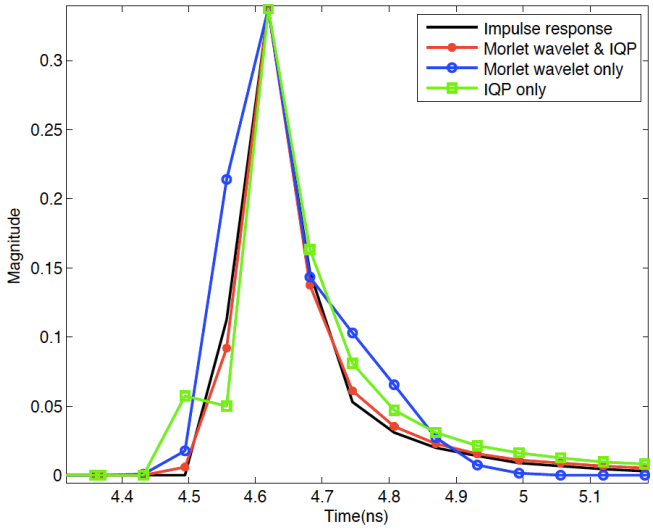

(a) Zoom-in of the first wave.

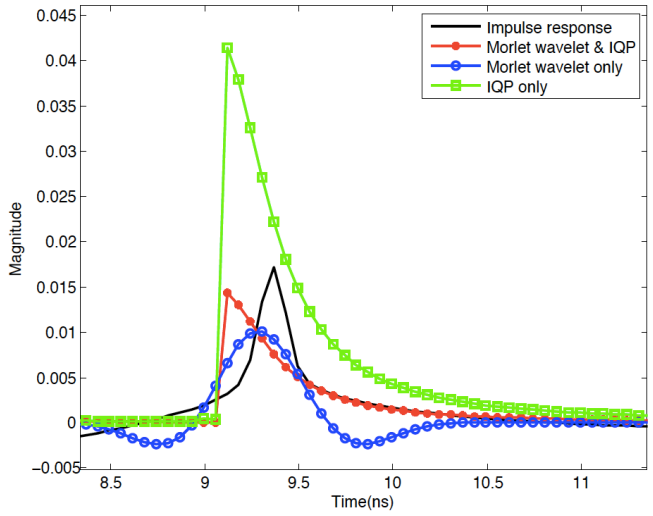

(b) Zoom-in of the second wave.

Fig. 5: Impulse response of the mismatched test case.

The result of our test case is presented in Figure 4. We illustrate the original impulse response signal in blue line, our reconstructed impulse response in green line, and impulse response by the inverse Fourier transform (IFT) in red dotted line. The original signal shows two sequential peaks, which are recovered by both the IFT and the our wavelets approximation method.

Our wavelets approximation method captures the delay of the first peak, and the causality constraints is satisfied within the error of the original signal, which is poorly captured by the IFT. The second peak is recovered with a shorter delay compared to the original signal. In the meanwhile, the magnitudes ratio for the two peaks are properly preserved, compared to the IFT method. The recovery error based on our method is much smaller than the recovery error based on the

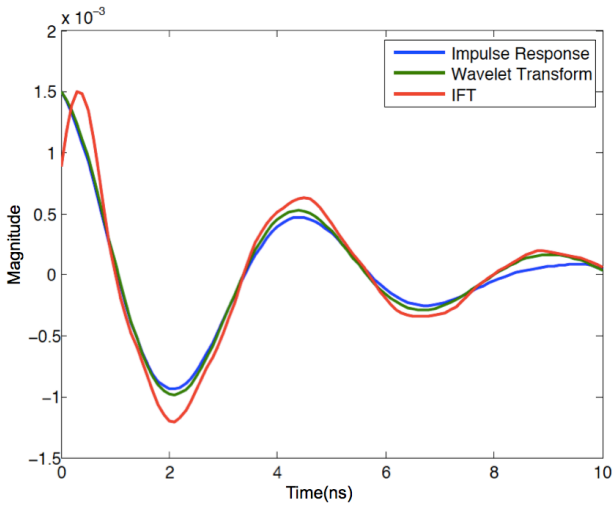

Fig. 6: Impulse response of the PDN.

IFT. Due to the bandwidth-limited spectrum, the IFT cannot precisely generate the original impulse response, especially in respect of the magnitude of peak values and the causal issue. The impulse response including reflection effects is usually non-trivial to be recovered by the conventional approximation approaches such as the rational functions. In summary, our proposed method simulates time-domain multi-reflections of impulse response accurately. Our simulation result reasonably meets causality because the time delay and captures the delay properly.

2) Simple Power Distribution Network: Figure 6 shows the result of our proposed compressed sensing method compared with the inverse Fourier transform of S_{11}.

Our method takes use of compressed sensing technique, thus relies on less frequency data. In contrast, although the invert Fourier transform produces the result as accurate as our method, IFT relies on the complete set of the frequency data which is usually unavailable for practical application. Furthermore, we observe that there exists a singular point at the time 0 because the frequency domain data, S_{11} of the PDN, are almost -1, of which the corresponding time domain result is an negative impulse at $t = 0$. In this test case, our method simply utilizes a small fraction of the frequency domain information, 300 points out of ten thousand frequency points.

V. Conclusion

In this paper, we have proposed a compressed sensing based method for incorporating the S-parameters to generate the impulse response in the time domain. We select two sets of the wavelet as the bases. We demonstrate that the combination of the sets produces better results in test cases. The method is intrinsically causal and stable by the problem formulation. The minimization of $L1$ norm mitigates the passivity issues. We also demonstrate that the method finds the internal reflection wave with proper delay. Further research is needed to enforce the passivity, and ensure the causality when the propagation delay is not known.

VI. Acknowledgement

We acknowledge the support of NSF CCF-1017864. We would like to acknowledge Dr. Bruce W. McGaughy and the ProPlus R&D team for introducing the project and technical discussion.

References

[1] T. J. Brazil, "Causal-Convolution – A New Method for the Transient Analysis of Linear Systems at Microwave Frequencies", *IEEE Trans. on Microwave Theory and Techniques*, 43(2) (1995), pp. 315-323.

[2] T. J. Brazil, "Accurate and Efficient Incorporation of Frequency-Domain Data within Linear and Non-linear Time-Domain Transient Simulation", *Proc. IEEE MTT-S International Microwave Symposium Digest*, 2005, pp. 797-800.

[3] E. J. Candès, J. K. Romberg and T. Tao, "Stable Signal Recovery from Incomplete and Inaccurate Measurement", *Communications on Pure and Applied Mathematics*, 59(8) (2006), pp. 1207-1223.

[4] E. J. Candès and M. B. Wakin, "An Introduction to Compressive Sampling", *IEEE Signal Processing Magazine*, 25(2) (2008), pp. 21-30.

[5] D. L. Donoho, "Compressed Sensing", *IEEE Trans. on Information Theory*, 52(4) (2006), pp. 1289-1306.

[6] B. Efron, T. Hastie, I. Johnstone and R. Tibshirani, "Least Angle Regression", *The Annals of Statistics*, 32(2) (2004), pp. 407-499.

[7] W.-D. Guo, J.-H. Lin, T.-W. Huang and R.-B Wu, "Fast Methodology for Determining Eye Diagram Characteristics of Lossy Transmission Lines", *IEEE Trans. on Advanced Packaging*, 32(1) (2009), pp. 175-183.

[8] S. H. Hall and H. L. Heck, *Advanced Signal Integrity for High-Speed Digital Designs*, Wiley, 2009.

[9] J. Lin and L. Qu, "Feature Extraction Based on Morlet Wavelet and Its Application for Mechanical Fault Diagnosis" *Journal of Sound and Vibration*, 234(1) (2000), pp. 135-148.

[10] A. V. Oppenheim, A. S. Willsky and S. H. Nawab, *Signals and Systems*, Prentice Hall, 2nd Edition, 1996.

[11] H. Peng and C.-K. Cheng, "Fast Transient Simulation of Lossy Transmission Lines", *Proc. ISCAS*, 2007, pp. 2706-2709.

[12] F. Rao, "Optimization of Spectrum Extrapolation for Causal Impulse Response Calculation Using the Hilbert Transform", U.S. Patent 7962541, Jun. 2011.

[13] P. Triverio, S. Grivet-Talocia, M. S. Nakhla, F. G. Canavero and R. Achar, "Stability, Causality, and Passivity in Electrical Interconnect Models", *IEEE Trans. on Advanced Packaging*, 30(4) (2007), pp. 795-808.

[14] Advanced Design System, *Keysight Technologies Inc.*, http://www.keysight.com

[15] MATLAB Code for the LARS Algorithm, http://publish.illinois.edu/xiaohuichen/code/lars

[16] Touchstone® File Format Specification Version 2.0, http://www.vhdl.org/ibis/touchstone_ver2.0/touchstone_ver2_0.pdf